



Contents lists available at ScienceDirect

Journal of Quantitative Spectroscopy & Radiative Transfer

journal homepage: www.elsevier.com/locate/jqsrt

The choice of optimal absorption coefficient in the Rank-Correlated SLW model for prediction of radiative transfer in high temperature gases

Brent W. Webb^{a,*}, Vladimir P. Solovjov^a, Frederic André^b^a Brigham Young University, 360 G EB, Provo, UT 84602, United States^b CNRS, INSA-Lyon, Université Claude Bernard Lyon 1, CETHIL, 5008 Villeurbanne, France

ARTICLE INFO

Article history:

Received 28 July 2021

Revised 20 October 2021

Accepted 21 October 2021

Available online 25 October 2021

Keywords:

Gas radiation

Rank correlated SLW model

ABSTRACT

The choice of gray gas absorption coefficient in the Rank Correlated Spectral Line Weighted-sum-of-gray-gases (RC-SLW) model is investigated. Several options are considered for calculating the gray gas absorption cross-section from the bounding supplemental absorption cross-sections, including that determined by inversion of the F -variable using Gauss Quadratures, the Geometric Mean of the bounding values, the Arithmetic Mean, and finally, a value determined from the weighting of the bounding supplemental absorption cross-sections using a variable interval fraction f . It is shown that an optimal value of the gray gas absorption coefficient can only be determined by accounting for the path length L . However, test cases and theoretical confirmation reveal that the Geometric Mean of the bounding supplemental absorption cross-sections for the gray gas absorption coefficient is the preferred method. The Geometric Mean approach is also nominally twice as fast computationally as the Gauss Quadrature approach used in the original RC-SLW model formulation. Therefore, this approach may be viewed as an enhancement to the model.

© 2021 Elsevier Ltd. All rights reserved.

1. Introduction to SLW correlated methods

The SLW method in its various forms, the Rank Correlated SLW method (RC-SLW), the Locally Correlated SLW method (LC-SLW), and the SLW Reference Approach (RA-SLW), are computationally efficient global methods for modeling of radiation transfer in non-uniform gaseous media. Their description and detailed construction can be found elsewhere [1–3]. The main idea behind the SLW method is representation of the continuous gas absorption spectrum by a histogram spectrum with just a few values of absorption coefficient (gray gas absorption coefficients) and their weights defined by their contribution to the total radiation transfer. Prediction accuracy using the model depends on the number of gray gases used.

Of the eight possible versions of the correlated SLW model [1], it has been shown that only the RC-SLW spectral model does not require specification of a gas reference thermodynamic state for its construction. Further, the RC-SLW model consists of the fewest steps in its construction. However, it was discovered that despite

the simplicity, robustness, and accuracy of the RC-SLW model, the CPU time associated with its application is noticeably higher than that of the RA-SLW and LC-SLW methods [4]. Construction of the SLW models is based on application of the Absorption-Line Blackbody Distribution Function (ALBDF), which is calculated in advance from the high-resolution gas absorption spectrum, and stored in tabulated form [5]. Both the direct ALBDF and its inverse are used in construction of the spectral models. Inversion of the ALBDF stored in tabulated form using multi-linear interpolation requires about six times more CPU time than the calculation of the direct ALBDF. Because the RC-SLW method requires more calculations of the inverse ALBDF than other correlated SLW methods, the total CPU time associated with application of the RC-SLW method is greater. Discretization into gray gases in the RC-SLW spectral model is based on application of nodes and weights of Gauss-Legendre integral quadratures. The boundaries of the intervals defined by the weights and nodes are involved in calculating the local absorption cross-sections through inversion of the ALBDF. However, because the role of the quadrature weights and the nodes are different, modifications of the RC-SLW method are explored here which reduce the number of inversions of the ALBDF, enhancing the computational efficiency of the RC-SLW method. The effect of these modifications on the predictive accuracy is also investigated.

* Corresponding author.

E-mail address: webb@byu.edu (B.W. Webb).

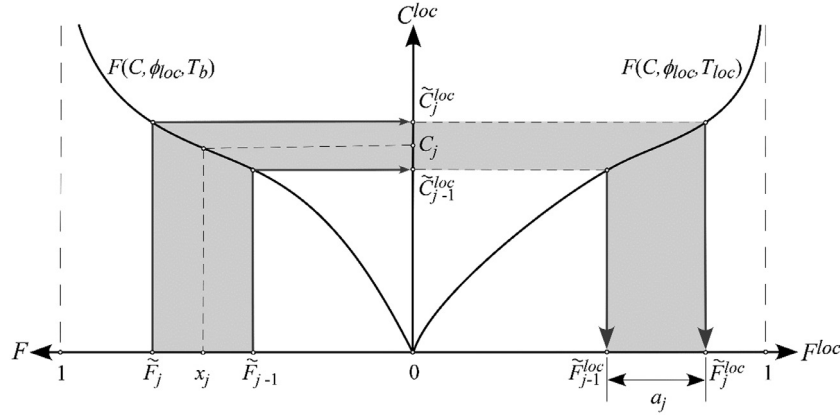


Fig. 1. Construction of the original formulation of the RC-SLW model.

Construction of the RC-SLW model

SLW correlated methods are based on the assumption of correlated/comonotonic gas absorption cross-section in non-uniform medium [3]. The construction of the spectral model for the RC-SLW model has been described in detail elsewhere (Solovjov et al., 2017). The details of construction of the original formulation of the RC-SLW model is shown graphically in Fig. 1. The sequence of calculation steps for determining the gray gas absorption coefficients and corresponding gray gas weights for the RC-SLW model may be summarized as follows:

- 1) Define partition of the F -variable for the full range $F \in [0, 1]$ into supplemental reference values:

$$\tilde{F}_0 = 0 \text{ and } \tilde{F}_j = \sum_{k=1}^j w_k \quad (1)$$

$$F_j = x_j, \quad j = 1, 2, \dots, n \quad (2)$$

where $x_j > 0$ are the positive abscissa (nodes) and $w_j, j = 1, 2, \dots, n$ are the corresponding weights of the Gaussian-Legendre quadrature for integration over the interval $[-1, 1]$.

- 2) Determine the local partition of the C -variable by inversion of the ALBDF:

$$\begin{aligned} \tilde{C}_j^{loc} &= C(\tilde{F}_j, \phi_{loc}, T_b), \quad j = 0, 1, \dots, n \text{ and} \\ C_j &= C(F_j, \phi_{loc}, T_b), \quad j = 1, 2, \dots, n \end{aligned} \quad (3)$$

- 3) Calculate the local gray gas coefficients:

$$\kappa_j = N^{loc} Y^{loc} C_j, \quad j = 1, 2, \dots, n \quad (4)$$

where N^{loc} is the local gas molar density and Y^{loc} is the local gas mole fraction.

- 4) Determine the gray gas weights using the direct ALBDF at the local cross-sections \tilde{C}_j^{loc} :

$$a_j = F(\tilde{C}_j^{loc}, \phi_{loc}, T_{loc}) - F(\tilde{C}_{j-1}^{loc}, \phi_{loc}, T_{loc}), \quad j = 1, 2, \dots, n \quad (5)$$

- 5) Finally, solve the local gray gas RTEs for the gray gas intensities I_j :

$$\frac{\partial I_j(s)}{\partial s} = -\kappa_j(s) I_j(s) + \kappa_j(s) a_j(s) I_b[T(s)], \quad j = 1, 2, \dots, n \quad (6)$$

The total radiation intensities are then found by summation over all gray gases $I = \sum_{j=1}^n I_j$.

The possible modifications of the RC-SLW model explored in this study are centered on the determination of the gray gas absorption coefficient (or gray gas absorption cross-section, C_j) outlined in step (2). In principle, rather than the nodal value x_j used in the Gauss-Legendre quadrature, any arbitrary value F_j may be chosen in the interval of supplemental values \tilde{F}_{j-1} and \tilde{F}_j . The corresponding gray gas absorption cross-section C_j is then determined by inverting the ALBDF at this arbitrary value F_j . Alternatively, C_j may be chosen as some weighted average of the local supplemental absorption cross sections \tilde{C}_{j-1} and \tilde{C}_j , bypassing the need to invert the ALBDF altogether. Modifications to the original formulation of the RC-SLW Model are investigated through four possible approaches, outlined here.

Gauss Quadrature (Original formulation)

As outlined previously, in the original formulation of the RC-SLW method, the local value of the gray gas absorption cross-sections C_j are calculated using the inverse ALBDF at the nodes of the Gaussian Quadratures (GQ) F_j as

$$C_j^{loc} = C(F_j, \phi_{loc}, T_b) \quad (7)$$

In the Gauss Quadrature approach, three inversions of the ALBDF are required for each gray gas. In practice, this may be reduced to two inversions since the inversion of \tilde{F}_{j-1} to find \tilde{C}_{j-1}^{loc} will have already been done for the previous gray gas as the gray gases are sequenced. The Gauss Quadrature approach will serve as the basis for comparison of the other modification approaches described next.

Geometric Mean

The second approach involves calculation of the local value of the gray gas absorption cross-sections C_j as the Geometric Mean (GM) of the bounding supplemental local absorption cross-sections \tilde{C}_j^{loc} which are determined at step (2) of construction of the RC-SLW spectral model

$$C_j = \sqrt{\tilde{C}_{j-1}^{loc} \tilde{C}_j^{loc}} \quad (8)$$

The Geometric Mean approach avoids the additional inversion of the ALBDF at the nodal value x_j required in the original Gauss Quadrature formulation of the RC-SLW model.

Arithmetic Mean

Another possible way to calculate the local values of absorption cross-sections C_j is the Arithmetic Mean (AM) of the bounding

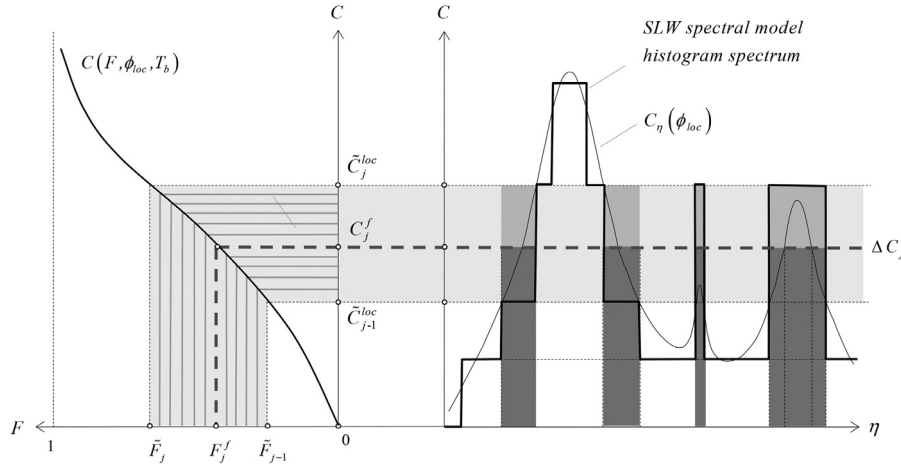


Fig. 2. Partition of the local C -variable into the set of supplemental absorption cross-sections \tilde{C}_j^{loc} for use in finding the gray gas absorption cross-section (absorption coefficient).

supplemental absorption cross-sections \tilde{C}_j^{loc} as

$$C_j = (\tilde{C}_{j-1}^{loc} + \tilde{C}_j^{loc})/2 \quad (9)$$

Similar to the Geometric Mean approach, calculating the gray gas absorption cross-section using the Arithmetic Mean avoids the additional inversion of the ALBDF at nodal value x_j required in the original RC-SLW model Gauss Quadrature formulation.

Variable Interval Fraction

One may designate an arbitrary value of F_j as a fraction f of the interval between the bounding supplemental ALBDFs from \tilde{F}_{j-1} to \tilde{F}_j . The local absorption cross-section in the corresponding range $\tilde{C}_{j-1}^{loc} \leq C_j \leq \tilde{C}_j^{loc}$ for the entire interval of gray gas absorption cross-sections may be determined using the set of cross-sections C_j^m

$$\tilde{C}_{j-1}^{loc} \leq C_j^m \leq \tilde{C}_j^{loc}, m = 0, 1, \dots, M \quad (10)$$

This set of cross-sections is convenient to generate using the Variable Interval Fraction approach by a uniform subdivision of the gray gas interval $\Delta F_j = \tilde{F}_j - \tilde{F}_{j-1}$

$$F_j^m = \tilde{F}_{j-1} + \frac{m}{M}(\tilde{F}_j - \tilde{F}_{j-1}) \quad (11)$$

where M is the number of points in the interval subdivision, or more simply in terms of the interval fraction f

$$F_j^f = \tilde{F}_{j-1} + f(\tilde{F}_j - \tilde{F}_{j-1}) \quad (12)$$

For a uniform subdivision in the interval $\tilde{C}_{j-1}^{loc} \leq C_j^m \leq \tilde{C}_j^{loc}$, the fraction becomes $f = m/M$. Then the local absorption cross-sections of the gray gases are found using the Inverse ALBDF as

$$C_j^m = C(F_j^m, \phi_{loc}, T_b) \quad (13)$$

$$C_j^f = C(F_j^f, \phi_{loc}, T_b) \quad (14)$$

This subdivision of the gray gas intervals is shown graphically in Fig. 2, where it is seen that the value of the local absorption cross-section C_j can lie anywhere between \tilde{C}_{j-1}^{loc} and \tilde{C}_j^{loc} . This defines the magnitude of the histogram absorption spectrum (shaded by the darkest gray in the figure). The choice of different absorption cross-sections C_j^f yields a different shape of the histogram absorption spectrum in the SLW model construction. The lowest values of C_j^f (for $f \rightarrow 0$) reduce or eliminate the peaks of the spectral lines, giving greater weight to the wings of the spectral lines.

The ALBDF variable F_j thus varies continuously in the interval as a function of the interval fraction f . Once a value of the interval fraction f has been selected, the value of F_j is used in the inversion of the ALBDF to determine C_j . This Variable Interval Fraction approach requires the additional inversion of the ALBDF and thus represents no improvement in computational efficiency relative to the original formulation of the RC-SLW model. However, this Variable Interval Fraction approach will permit the systematic exploration of a possible optimal value of the absorption cross-section.

2. RC-SLW model predictions

Three test cases with large gas temperature variation are used here to compare the performance of the different approaches outlined in the foregoing section for evaluating the gray gas absorption cross-section. These test cases consider both emission-dominated and absorption-dominated scenarios in the gas medium. For the emission-dominated cases, the volume-average gas emission (volume-average of the product of the Planck mean absorption coefficient and the blackbody emission at the gas temperature) exceeds the volume-average gas absorption (volume-average of the product of the Planck mean absorption coefficient and the blackbody emission at the wall temperature), and the reverse is true for the absorption-dominated case. In most cases, emission-dominated scenarios are those for which the gas temperature is higher than that of the walls, and absorption-dominated cases are for those situations where the walls are hotter than the gas.

Consider radiative transfer in a plane-parallel layer bounded by black walls and filled with a mixture of water vapor and carbon dioxide (remainder nitrogen). RC-SLW model and line-by-line benchmark solutions were carried out with the Multi-Layer analytical method [6] using 100 spatial increments in the layer. The SLW multiplication approach was used for modeling the gas mixture as a single gas [7], and the ALBDF tabulated in Pearson et al. [5] was used. In all test cases studied here, the blackbody source temperature was taken as the volume-average temperature of the medium, $T_b = T_{ave}$. Predictions were made for the three test cases using the Gauss Quadrature, Geometric Mean, Arithmetic Mean, and Variable Interval Fraction approaches for calculating the gray gas absorption cross-section. Results were generated for different number of gray gases, n , in the spectral model, and for different values of the interval fraction f used in the Variable Interval Fraction approach.

The temperature and gas species mole fraction profiles for Test 1 and Test 2 are given by

$$T(x) = T_{\min} + (T_{\max} - T_{\min}) \sin(\pi x/L) \quad (15a)$$

$$Y_{\text{H}_2\text{O}}(x) = Y_{\min} + (Y_{\max} - Y_{\min}) \sin(\pi x/L) \quad (15b)$$

$$Y_{\text{CO}_2}(x) = Y_{\text{H}_2\text{O}}(x)/2 \quad (15c)$$

where the values of T_{\min} , T_{\max} , Y_{\min} , and Y_{\max} are specified for the test cases. Hereafter, the Total Relative Error is defined as the local absolute error relative to the line-by-line benchmark solution integrated over the layer width, normalized by the integrated total flux divergence for the benchmark prediction.

Test 1. In this test case the following parameters are used: $L = 1$ m, $T_{\min} = 500$ K, $T_{\max} = 2000$ K, $T_{\max} - T_{\min} = 1500$ K, $Y_{\min} = 0.2$, $Y_{\max} - Y_{\min} = 0.2$. The predicted local total radiative flux divergence using the GQ, GM, AM, and $f = 0$ approaches defined above for determining the gray gas absorption coefficient for $n = 25$ gray gases is shown in Fig. 3a. The figure also shows the line-by-line (LBL) benchmark solution. Fig. 3b shows the dependence of the Total Relative Error on the value of interval fraction f used to determine the gray gas absorption coefficient for the number of gray gases ranging from $n = 5$ to 25, and Fig. 3c illustrates the dependence of the predictive accuracy on the number of gray gases for the GQ, GM, AM, and $f = 0$ approaches.

Fig. 3a reveals that all methods yield reasonable engineering accuracy in the prediction of the local radiative flux divergence. Some modest error in the GQ, GM and AM predictions is noted in the center of the layer where the highest temperatures are found. Quite surprisingly, the prediction for $f = 0$ is nearly indistinguishable from the line-by-line benchmark solution.

Fig. 3b shows generally that the Total Relative Error for all values of f decreases as the number of gray gases is increased. This is to be expected, since an increase in n captures more accurately the variations in the gas absorption spectrum. Fig. 3b also reveals, generally, that the maximum total error occurs for $f = 0$ and $f = 1$, corresponding to $C_j = \tilde{C}_{j-1}$ and $C_j = \tilde{C}_j$, respectively. A local minimum in the error is noted at some intermediate value of f for all values of n studied, and that intermediate value is observed to be approximately $f < 0.4$. The value of the interval fraction f at which the total error reaches its minimum is dependent on the number of gray gases used, and that value of f decreases with increasing n . The figure shows, further, that as n is increased, the dependence of the Total Relative Error on f decreases. Indeed, predictions reveal that for $n > 100$ the total error is nearly independent of f . This is to be expected, since for $n \rightarrow \infty$, the RC-SLW method approaches its continuous limit given by the Generalized SLW model [8], and the difference between the bounding supplemental gray gas absorption coefficients vanishes $\tilde{C}_j - \tilde{C}_{j-1} \rightarrow 0$. Therefore, the value of $C_j^{\text{loc}} \rightarrow \tilde{C}_j \approx \tilde{C}_{j-1}$.

Fig. 3c reveals that the accuracy of the approach to determining the gray gas absorption cross-section is quite sensitive to the value of gray gas absorption coefficient in the interval $[\tilde{C}_{j-1}, \tilde{C}_j]$ used in the predictions. Consistent with the results of Fig. 3a, the $f = 0$ predictions (for which $C_j = \tilde{C}_{j-1}$) in Fig. 3c show a decrease in error with increasing n for $n < 25$ gray gases. The Total Relative Error for the Gauss Quadrature, Geometric Mean, and Arithmetic Mean approaches show little dependence on n for $n > 8 - 10$. The value of minimum error for $n \rightarrow \infty$ is finite, and subject to the correlated spectrum assumption underlying the RC-SLW method. Also shown in Fig. 3c are predictions for $n = 128$ gray gases for the GQ, GM, AM, and $f = 0$ approaches. These predictions reveal that all methods for calculating the gray gas absorption cross-section approach

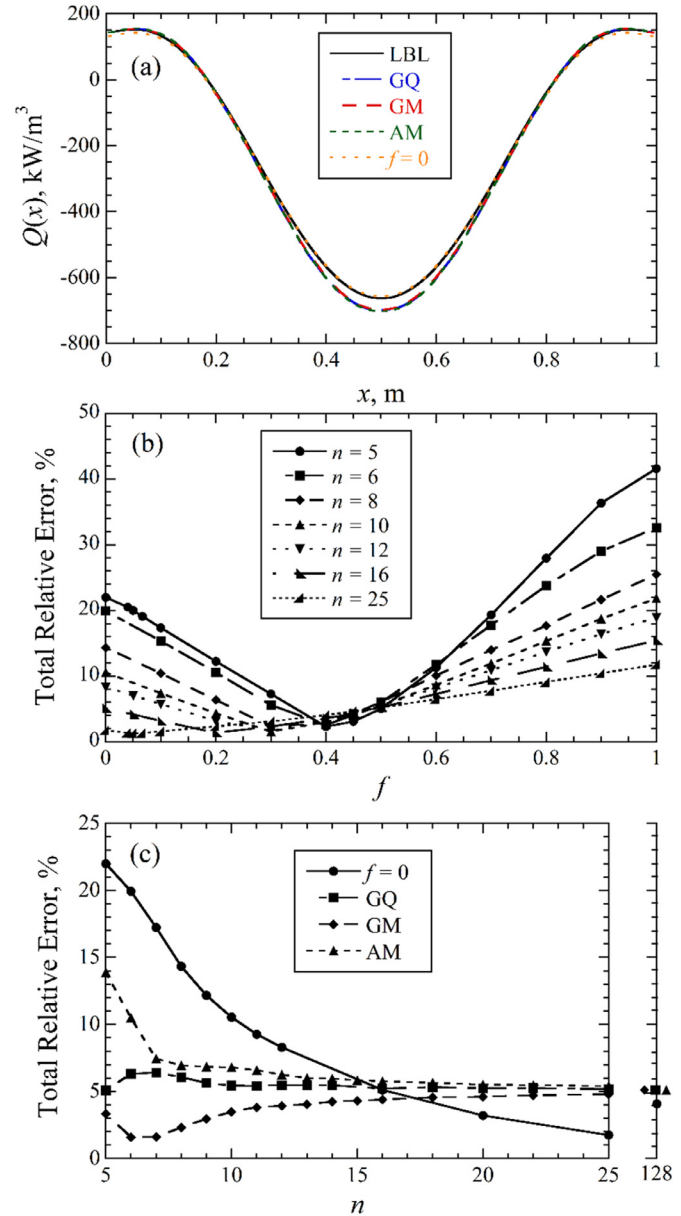


Fig. 3. Predictions for Test 1: a) Total divergence of the net radiative flux for $n = 25$, b) Total Relative Error as a function of interval fraction f , and c) Total Relative Error as a function of number of gray gases n .

the same Total Relative Error as $n \rightarrow \infty$. For this test case, nearly line-by-line accuracy is achieved (with Total Relative Error $< 1\%$) for $f = 0$ at $n \approx 6$, but the error increases as n is further increased (shown by the data for $n = 128$). This indicates that the $f = 0$ approach exhibits a local minimum in Total Relative Error with increasing n , similar to the Geometric Mean Approach (for which the minimum total error occurs for $n \approx 6 - 7$). Interestingly, the Geometric Mean approach yields accuracy for $n \approx 6$ that rivals that of the $f = 0$ approach for $n = 25$. This non-monotonic dependence of total error on number of gray gases for the RC-SLW model, particularly at low values of n , has been reported previously [9].

Table 1 summarizes the Total Relative Error for the four different approaches used in Test 1 with number of gray gases $n = 5, 25, \text{ and } 128$. Consistent with the results shown in Fig. 3, the accuracy of the $f = 0$ approach increases as n increases from 5 to

Table 1

Total Relative Error,%, for the four different approaches used in Test 1 for calculating the gray gas absorption coefficient, GQ, GM, AM, and $f = 0$.

Approach	$n = 5$	$n = 25$	$n = 128$
Gaussian Quadrature	5.1	5.2	5.2
Geometric Mean	3.4	4.8	5.1
Arithmetic Mean	13.9	5.4	5.2
$f = 0$	22.0	1.7	4.0

Table 2

Total Relative Error,%, for the four different approaches used in Test 2 for calculating the gray gas absorption coefficient, GQ, GM, AM, and $f = 0$.

Approach	$n = 5$	$n = 25$	$n = 128$
Gaussian Quadrature	7.7	7.0	7.0
Geometric Mean	4.5	6.5	6.9
Arithmetic Mean	14.5	7.2	7.0
$f = 0$	22.3	1.9	5.7

25 gray gases. As noted previously, the dependence of the accuracy on the value of f is expected to decrease as the number gray gases increases. Among all of the approaches studied for determining C_j , the Arithmetic Mean approach yields generally the worst accuracy, with Total Relative Error that can exceed 10%. The Geometric Mean approach yields arguably the best overall accuracy over the range of n explored, and is particularly accurate for a small number of gray gases. The Geometric Mean approach is thus particularly attractive for engineering radiative transfer predictions, where a small number of gray gases would likely be employed.

Test 2. The second test is identical to the first with the exception that a larger gas temperature and gas species mole fraction variation is imposed in the layer. The following parameters are used for Test 2: $L = 1$ m, $T_{\min} = 500$ K, $T_{\max} = 2500$ K, $T_{\max} - T_{\min} = 2000$ K, $Y_{\min} = 0.2$, $Y_{\max} - Y_{\min} = 0.4$. Results are shown in Fig. 4. The predicted local total radiative flux divergence using the GQ, GM, AM approaches, and the prediction with $f = 0$ for $n = 25$ is shown in Fig. 4a, along with the LBL solution. Fig. 4b shows the dependence of the Total Relative Error on the interval fraction f used to determine the gray gas absorption coefficient for a range of n , and Fig. 4c illustrates the dependence of the predictive accuracy on the number of gray gases for the GQ, GM, AM, and $f = 0$ approaches. Behavior similar to that observed in Fig. 3 for Test 1 is also found in the predictions for Test 2, with very little increase in error despite the significantly larger imposed gas temperature and species mole fraction differences in the layer. Fig. 4c again confirms that predictions for all methods (GQ, GM, AM, and $f = 0$) approach the same Total Relative Error as n increases, and that both the Geometric Mean and $f = 0$ approaches exhibit a local minimum in the total error dependence on n . For this test case, the local minimum in error for $f = 0$ occurs for $n \approx 23$ gray gases.

Table 2 summarizes the Total Relative Error for the four different approaches used in Test 2 with $n = 5, 25$, and 128. As with Test 1, and consistent with the results shown previously in Fig. 4, the zero interval fraction $f = 0$ approach yields improved accuracy as n increases (and predictions would be expected to be entirely independent of f as $n \rightarrow \infty$). The agreement with the line-by-line benchmark for $f = 0$ is remarkable for this test case, given the wide variation in gas temperature. As with Test 1, the Geometric Mean approach yields perhaps the best overall accuracy over the range of n explored.

The following general observations may be made relative to the emission-dominated cases of Test 1 and Test 2. It is seen that the accuracy of the predictions is sensitive to the choice of the gray gas

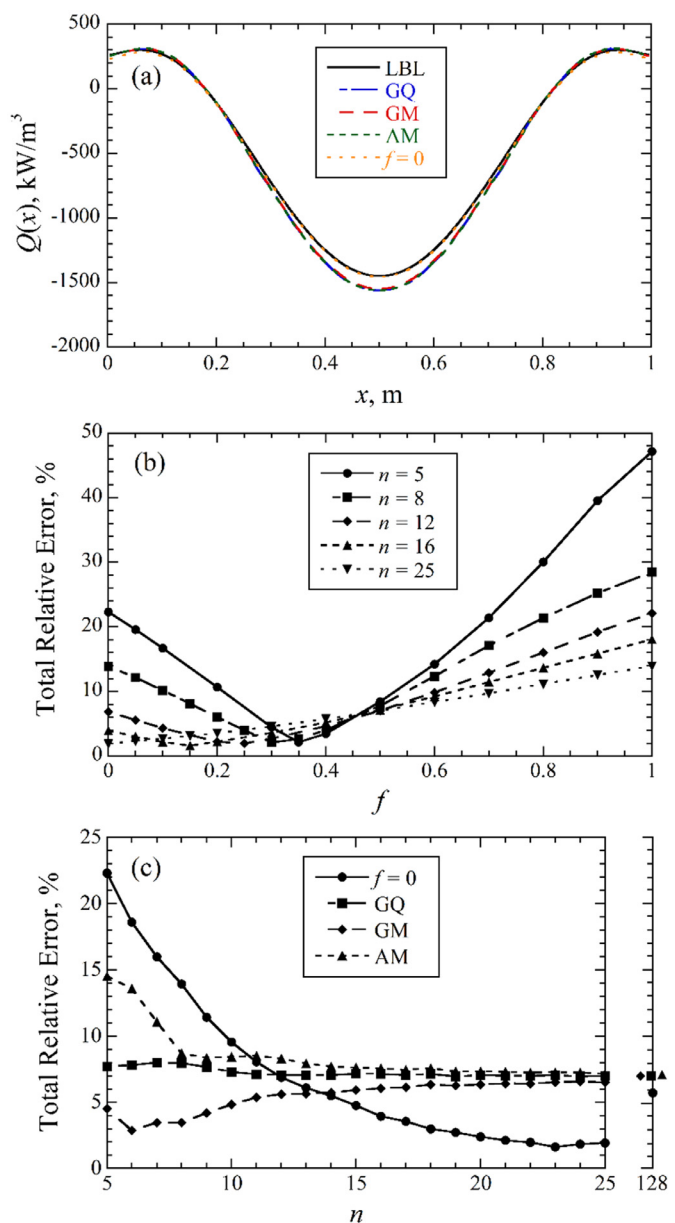


Fig. 4. Predictions for Test 2: a) Total divergence of the net radiative flux for $n = 25$, b) Total Relative Error as a function of interval fraction f , and c) Total Relative Error as a function of number of gray gases n .

interval fraction f . For $n = 5$, the minimum error is obtained for an approximate value $f = 0.4$ in Test 1, and $f = 0.35$ in Test 2. With an increase in the number of gray gases, the predictive accuracy becomes less dependent on the value of f .

The results of the foregoing tests reveal, surprisingly, that the prediction accuracy using $f = 0$ at its minimum total error surpasses that of all other approaches, and the prediction becomes almost indistinguishable from the LBL solution at intermediate values of n , even for the extreme temperature difference of Test 2, $T_{\max} - T_{\min} = 2000$ K. It must be acknowledged, however, that this observation cannot be generalized for all possible prediction scenarios.

For the small number of gray gases used in practical engineering calculations, the error prediction in the Arithmetic Mean approach for determining the absorption cross-section is very large, and it falls with an increase of the number of gray gases, approach-

Table 3

Total Relative Error,%, for the four different approaches used in Test 3 for calculating the gray gas absorption coefficient, GQ, GM, AM, and $f = 0.45$.

Approach	$n = 5$	$n = 25$
Gaussian Quadrature	11.2	10.0
Geometric Mean	14.0	9.7
Arithmetic Mean	26.2	10.1
$f = 0.45$	10.6	9.9

ing the error found for the Gaussian Quadrature and Geometric Mean approaches. Finally, the results of Tests 1 and 2 suggest that the predictive accuracy using the Geometric Mean approach for determining the gray gas absorption cross-section yields the best accuracy for a small number of gray gases, and in general (for these test cases studied), yields more accurate predictions than using the more computationally costly Gauss Quadrature approach of the original RC-SLW model formulation for any number of gray gases.

Test 3. In contrast to the previous two test cases where gas emission was dominant relative to absorption, Test 3 presents a case where gas absorption is dominant in the radiative transfer. The following hyperbolic temperature and mole fraction profiles are imposed in the layer for Test 3:

$$T(x) = \frac{T_{\min} + T_{\max}}{2} + \frac{T_{\max} - T_{\min}}{2} \left(1 - \frac{2x}{L}\right)^3 \tag{16a}$$

$$Y_{\text{H}_2\text{O}}(x) = \frac{Y_{\min} + Y_{\max}}{2} + \frac{Y_{\max} - Y_{\min}}{2} \left(1 - \frac{2x}{L}\right)^3 \tag{16b}$$

$$Y_{\text{CO}_2}(x) = Y_{\text{H}_2\text{O}}(x)/2 \tag{16c}$$

For this test case the maximum temperature is at the boundary, $x = 0$. The following parameters were used in Test 3: $L = 2$ m, $T_{\min} = 500$ K, $T_{\max} = 2500$ K, $T_{\max} - T_{\min} = 2000$ K, $Y_{\min} = 0.2$, $Y_{\max} = 0.4$, $Y_{\max} - Y_{\min} = 0.2$. Predictions are shown Fig. 5. Unlike the trends observed for Tests 1 and 2, Fig. 5a shows that the predictions for Test 3 using the GQ, GM, AM, and $f = 0.45$ approaches using $n = 25$ gray gases are very close to each other except at the right boundary. Consequently, none of the approaches for choosing the gray gas absorption coefficient considered adds significantly to the accuracy of the conventional Gauss Quadrature RC-SLW prediction except for a very small number of gray gases, n . The Total Relative Error for this test case, shown in Fig. 5b, is significantly higher for all approaches than for Tests 1 and 2. The reduced accuracy of the RC-SLW model in general for absorption-dominated scenarios has been documented previously [10]. As seen in Fig. 5b, the local minimum in Total Relative Error as a function of f appears at the same value of f (≈ 0.45) for all values of n . Further, Fig. 5b shows that the total error is nearly independent of interval fraction f for $n = 25$. Fig. 5c reveals that the Total Relative Error in the Gauss Quadrature and $f = 0.45$ Test 3 predictions is nearly independent of the number of gray gases, as is that of the Arithmetic Mean prediction for $n > 15$ and Geometric Mean prediction for $n > 7$. The Arithmetic Mean exhibits the largest error and the greatest dependence on the number of gray gases. Finally, the results of Test 3 reveal that for an increase in the number of gray gases, the influence of the choice of local absorption cross-section decreases.

Table 3 summarizes the Total Relative Error for the four different approaches used in Test 3 with $n = 5$ and 25. In contrast to the results of Tests 1 and 2, the four different approaches yield nearly the same accuracy with both $n = 5$ and 25. For this absorption-dominated case, it appears that no enhancement to the RC-SLW model accuracy can be achieved with any of the approaches for calculating the gray gas absorption coefficient. The

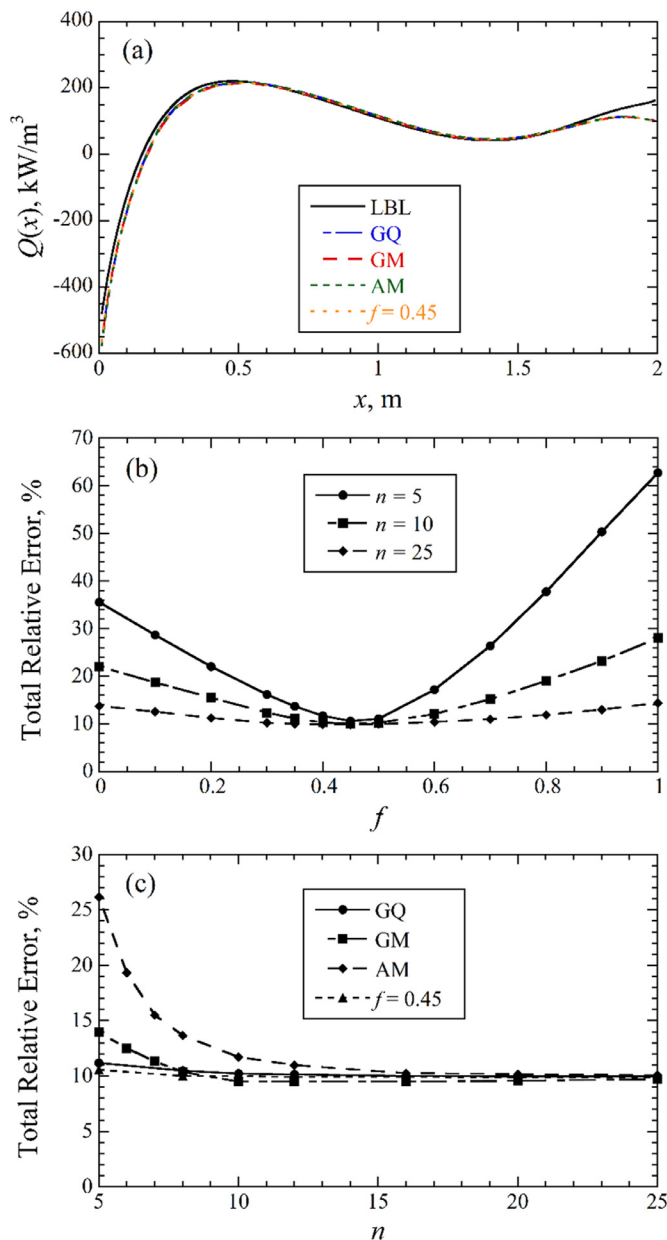


Fig. 5. Predictions for Test 3: a) Total divergence of the net radiative flux for $n = 25$, b) Total Relative Error as a function of interval fraction f , and c) Total Relative Error as a function of number of gray gases n .

relatively poorer accuracy and generally different behavior in Test 3 compared to Tests 1 and 2 is centered on the dominance of local gas absorption relative to gas emission in this problem. Indeed, as stated previously, the RC-SLW model in its original formulation is also seen to yield somewhat reduced accuracy in this problem, which has been observed previously [11].

The total CPU time for the simulations of Test 1 is shown in Fig. 6 for the Gauss Quadrature, Geometric Mean, and Arithmetic Mean approaches. The CPU time for the $f = 0$ approach (not shown) is nominally the same as that for the Arithmetic Mean approach. The CPU time results for Tests 2 and 3 are virtually the same as for Test 1.

It is noted in Fig. 6 that the computation time for the Geometric Mean and Arithmetic Mean approach is significantly lower than that for the Gauss Quadrature approach used in the original formulation of the RC-SLW model. This is the result of eliminating the

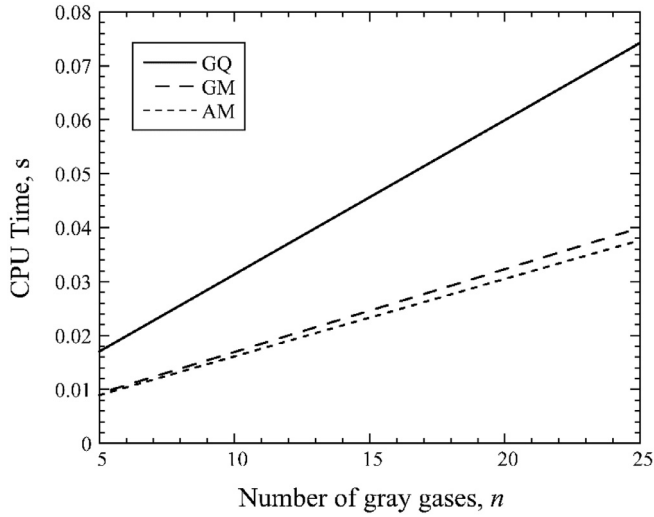


Fig. 6. Total CPU time for Test 1 as a function of number of gray gases for the Gauss Quadrature, Geometric Mean, and Arithmetic Mean approaches.

need for the additional inversion of the ALBDF of the nodal value x_j for each gray gas required in the original RC-SLW model formulation Gauss Quadrature approach. As stated previously, the ALBDF inversion is one of the most computationally costly steps in the RC-SLW spectral model construction. Fig. 6 shows that the computational savings for the Geometric Mean and Arithmetic Mean approaches is nearly a factor of two. This finding is significant given that the prediction of radiation transfer is invariably the most computationally demanding transport solution in a coupled modeling scenario. Thus, it appears that the Geometric Mean approach is preferable both from an accuracy perspective (at least for a small number of gray gases) and from the computation time perspective.

3. Estimating the optimal value of the gray gas absorption coefficient

The results of the test cases shown in the foregoing section demonstrate generally a decrease in the Total Relative Error for the prediction of the radiative net flux divergence with an increase in the number of gray gases. In addition, the predictions for Tests 1 and 2 reveal a reduction of the optimal interval fraction f with an increase of number of gray gases. This corresponds to the minimum Total Relative Error in the prediction of total flux divergence, while the optimal value of interval fraction for $n = 5$ is $f = 0.4$ in Test 1 and $f = 0.35$ for Test 2. There is a theoretical foundation for these observations, which is now developed.

One can apply the Generalized SLW approach [8] which permits the description of the SLW method in terms of the absorption coefficient because the detailed analysis in terms of absorption cross-section is not needed in further derivation. Using the original notation F for the Absorption Line Blackbody Distribution Function F -variable, $0 \leq F \leq 1$, the partition of F into its supplemental values \tilde{F}_j for $j = 1, 2, \dots, n$ defines the gray gases, $\tilde{F}_{j-1} \leq F_j \leq \tilde{F}_j$. Following the usual construction of the RC-SLW model, the local supplemental gray gas absorption coefficients are calculated with the help of the inverse ALBDF at the local thermodynamic state $\phi = \{P, T, Y_{H_2O}, Y_{CO_2}\}$ and at some blackbody source temperature T_b as the value of the cumulative k -distribution function

$$\tilde{k}_j = k(\tilde{F}_j, \phi, T_b) = NYC(\tilde{F}_j, \phi, T_b), j = 1, 2, \dots, n \quad (17)$$

The local supplemental values of the F -variable are then calculated using the ALBDF at the local thermodynamic state ϕ and the

local blackbody source temperature $T_b = T$ as

$$\tilde{F}_j^{loc} = F(\tilde{C}_j, \phi, T), j = 1, 2, \dots, n \quad (18)$$

which are used for calculation of the local gray gas weights

$$a_j = \tilde{F}_j^{loc} - \tilde{F}_{j-1}^{loc}, j = 1, 2, \dots, n \quad (19)$$

To complete the construction of the RC-SLW spectral model the local values of the gray gas absorption coefficients κ_j must be defined. In the original version of the RC-SLW model, they are calculated using the nodes of the Gauss-Legendre quadratures F_j as

$$\kappa_j = \kappa(F_j, \phi, T_b) = NYC(F_j, \phi, T_b), j = 1, 2, \dots, n \quad (20)$$

As stated previously, because this calculation requires inversion of the ALBDF, it is more computationally costly. One possibility to avoid this additional inversion of the ALBDF is to calculate the gray gas absorption coefficients from the bounding local supplemental absorption coefficients already defined using the Geometric Mean approach as

$$\kappa_j = \sqrt{\tilde{\kappa}_{j-1} \tilde{\kappa}_j} \quad (21)$$

Consider the total transmissivity of a gas isothermal homogeneous layer of thickness L . For simplicity, to avoid confusion between F and F^{loc} and the too-frequent use of the superscript loc , one can rename the local values F^{loc} as G . To further simplify, one may omit from the notation the dependence on ϕ and T_b in $\kappa(F, \phi, T_b)$, and use the continuous representation of the total transmissivity using the Generalized SLW method as [8]

$$\tau(L) = \int_0^1 e^{-\kappa(G)L} dG \quad (22)$$

Then the generalized SLW representation of the transmissivity is

$$\tau(L) = \sum_{j=1}^n \int_{G_{j-1}}^{G_j} e^{-\kappa(G)L} dG \quad (23)$$

For simplicity, one can write

$$G_{j-1} = F(\tilde{C}_{j-1}, \phi, T) \quad (24)$$

$$G_j = F(\tilde{C}_j, \phi, T) \quad (25)$$

Now consider the transmissivity of the j^{th} gray gas term

$$\tau_j(L) = \int_{G_{j-1}}^{G_j} e^{-\kappa(G)L} dG \quad (26)$$

According to the Mean Value Theorem, there exists a value G_L such that

$$\int_{G_{j-1}}^{G_j} e^{-\kappa(G)L} dG = (G_j - G_{j-1})e^{-\kappa(G_L)L} \quad (27)$$

Then

$$e^{-\kappa(G_L)L} = \frac{1}{(G_j - G_{j-1})} \int_{G_{j-1}}^{G_j} e^{-\kappa(G)L} dG \quad (28)$$

Now consider the graphical interpretation shown in Fig. 7. The corresponding value of the local j^{th} gray gas absorption coefficient is

$$\kappa_j = \kappa(G_L, \phi, T) \quad (29)$$

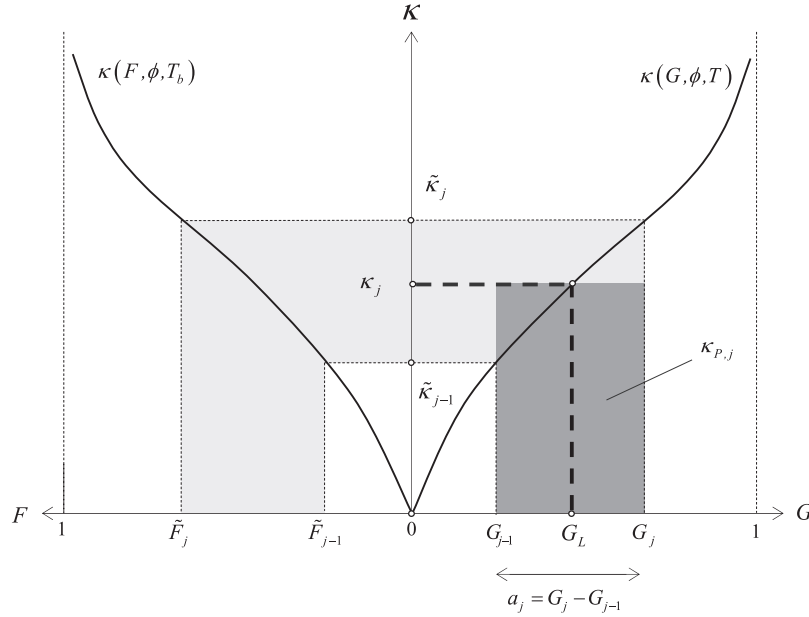


Fig. 7. The local gray gas absorption coefficient based on transmissivity of the gas layer (noting that $\kappa = \text{NYC}$).

Consider the gray gas transmissivity averaged over the interval $G_j - G_{j-1}$

$$\begin{aligned} & \frac{1}{G_j - G_{j-1}} \int_{G_{j-1}}^{G_j} e^{-\kappa(G)L} dG \\ &= e^{-\kappa(G_{j-1})L} \frac{1}{G_j - G_{j-1}} \int_{G_{j-1}}^{G_j} e^{-[\kappa(G) - \kappa(G_{j-1})]L} dG \\ &= \exp \left\{ -\kappa(G_{j-1})L + \ln \left[1 - \frac{1}{G_j - G_{j-1}} \int_{G_{j-1}}^{G_j} \left(1 - e^{-[\kappa(G) - \kappa(G_{j-1})]L} \right) dG \right] \right\} \end{aligned} \quad (30)$$

Now denote a variable ξ

$$\xi = \frac{1}{G_j - G_{j-1}} \int_{G_{j-1}}^{G_j} \left(1 - e^{-[\kappa(G) - \kappa(G_{j-1})]L} \right) dG \quad (31)$$

Following the derivation of André [12], it is seen that with a sufficient number of gray gases (or the practically irrelevant case of vanishing L), the term $[\kappa(G) - \kappa(G_{j-1})]L$ is small, and consequently, the value of $\xi \rightarrow 0$. The linear approximation near 0 can then be used, namely $\ln(1 - \xi) \approx -\xi$, yielding

$$\begin{aligned} & \frac{1}{G_j - G_{j-1}} \int_{G_{j-1}}^{G_j} e^{-\kappa(G)L} dG \\ &= \exp \left\{ -\kappa(G_{j-1})L - \frac{1}{G_j - G_{j-1}} \int_{G_{j-1}}^{G_j} \left(1 - e^{-[\kappa(G) - \kappa(G_{j-1})]L} \right) dG \right\} \\ &= e^{-[\kappa(G_{j-1})L - \xi]} \end{aligned} \quad (32)$$

With an increase in the number of gray gases and for moderate gas pathlengths, the difference between the gray gas absorption coefficients at the interval boundaries vanishes, yielding

$\kappa(G_j) - \kappa(G_{j-1}) \rightarrow 0$. Then, Eq. (32) reduces to

$$\begin{aligned} & \frac{1}{G_j - G_{j-1}} \int_{G_{j-1}}^{G_j} e^{-\kappa(G)L} dG \\ & \approx \exp \left[-\frac{L}{G_j - G_{j-1}} \int_{G_{j-1}}^{G_j} \kappa(G) dG \right] \approx e^{-\kappa(G_{j-1})L} \approx e^{-\kappa(G_j)L} \end{aligned} \quad (33)$$

This result confirms, not surprisingly, that the dependence of the optimal value G_L on the interval fraction f thus vanishes for $n \rightarrow \infty$. This finding is consistent with the predictions for all three test cases presented previously (Figs. 3–5), where the dependence of the Total Relative Error on f was found to decrease with an increase in the number of gray gases.

The optimal value of G_L in the limit of very large path length L may also be identified. Beginning with Eq. (28), the objective is to find the asymptotic limit of G_L for $L \rightarrow \infty$. Normalizing the variable of integration, Eq. (28) may be written as

$$e^{-\kappa(G_L)L} = \frac{1}{G_j - G_{j-1}} \int_{G_{j-1}}^{G_j} e^{-\kappa(G)L} dG = \int_0^1 e^{-\kappa(X)L} dX \quad (34)$$

The integral on the right-hand side of Eq. (34) may be written as a weighted sum (as, for example, a Lobatto quadrature in which the endpoint weight w_0 is not null):

$$\int_0^1 e^{-\kappa(X)L} dX = w_0 e^{-\kappa_{\min}L} + w_{n+1} e^{-\kappa_{\max}L} + \sum_{i=1}^n w_i e^{-\kappa(X_i)L} \quad (35)$$

where $\kappa_{\min} = \kappa(G_{j-1})$ and $\kappa_{\max} = \kappa(G_j)$. Eq. (35) may be written as

$$\begin{aligned} e^{-\kappa(G_L)L} &= \int_0^1 e^{-\kappa(X)L} dX = w_0 e^{-\kappa_{\min}L} \left[1 + \frac{w_{n+1}}{w_0} e^{-(\kappa_{\max} - \kappa_{\min})L} \right. \\ & \quad \left. + \sum_{i=1}^n \frac{w_i}{w_0} e^{-(\kappa(X_i) - \kappa_{\min})L} \right] \end{aligned} \quad (36)$$

Operating on the left-hand and right-hand sides of the equality in Eq. (36) by $-\ln$ (negative of the natural logarithm) and dividing by L yields:

$$\kappa(G_L) = \kappa_{\min} - \frac{1}{L} \ln(w_0) + \frac{1}{L} \ln \left[1 + \frac{w_{n+1}}{w_0} e^{-(\kappa_{\max} - \kappa_{\min}) L} + \sum_{i=1}^n \frac{w_i}{w_0} e^{-\kappa(X_i) L} \right] \quad (37)$$

In the limit as $L \rightarrow \infty$, Eq. (37) yields

$$\lim_{L \rightarrow \infty} \kappa(G_L) = \kappa_{\min} \quad (38)$$

Thus, for very large pathlength the optimal absorption coefficient is the minimum value in the interval $\kappa(G_L) = \kappa(G_{j-1})$, and this limit is independent of the number of gray gases used. This limiting behavior will be confirmed through alternate analysis in a section to follow.

3.1. Bounds for the optimal gray gas absorption coefficient

Although it was shown in the previous section that the dependence of optimal gray gas absorption coefficient in the interval $\tilde{\kappa}_{j-1} < \kappa_j < \tilde{\kappa}_j$ on interval fraction f decreases with an increase in the number of gray gases n , it would be useful to identify bounds on the optimal value in this interval for finite number of gray gases. Indeed, it is possible to determine theoretically the bounds on the optimal gray gas coefficient in this interval. Consider the j^{th} gray gas transmissivity of the pathlength L averaged over the interval $\Delta G = G_j - G_{j-1}$

$$\tau^{\Delta G}(L) = \frac{1}{\Delta G} \int_{\Delta G} e^{-\kappa(G)L} dG \quad (39)$$

The reordered absorption coefficient $\kappa(G) = \kappa(G, \phi, T)$ is a strictly increasing function of G from $\kappa(G_{j-1})$ to $\kappa(G_j)$. Therefore, for a given pathlength L

$$\tau^{\Delta G}(L) = \frac{1}{\Delta G} \int_{\Delta G} e^{-\kappa(G)L} dG \leq e^{-\kappa(G_{j-1})L} \quad (40)$$

This result is illustrated graphically in Fig. 8, where $e^{-\kappa(G_{j-1})L}$ is plotted a function of κ and G along with the relevant distributions $\kappa(F, \phi, T_b)$ and $\kappa(G, \phi, T)$.

Let G_L be the solution of the following implicit equation (which also has a unique solution)

$$\tau^{\Delta G}(L) = e^{-\kappa(G_L)L} \quad (41)$$

At this point it is useful to recall a mathematical statement termed Jensen's Inequality for a convex function Γ [13]

$$\Gamma \left[\frac{1}{\Delta G} \int_{\Delta G} f(G) dG \right] \leq \frac{1}{\Delta G} \int_{\Delta G} \Gamma[f(G)] dG \quad (42)$$

The exponential function $\Gamma(G) = e^{-\kappa(G)L}$ is a convex function with respect to the variable G , as seen in Fig. 8. Thus, for the continuous function $f(G) = e^{-\kappa(G)L}$ Jensen's inequality yields

$$\tau^{\Delta G}(L) = \frac{1}{\Delta G} \int_{\Delta G} e^{-\kappa(G)L} dG \geq e^{-\frac{1}{\Delta G} \int_{\Delta G} \kappa(G)L dG} = e^{-\kappa(G_p)L} \quad (43)$$

In Eq. (43), G_p is the solution of the implicit equation

$$\kappa(G_p) \Delta G = \int_{\Delta G} \kappa(G) dG \quad (44)$$

and

$$\int_{\Delta G} \kappa(G) dG = \kappa_p \Delta G \quad (45)$$

is the j^{th} gray gas Planck mean absorption coefficient. According to the Intermediate Value Theorem, Eq. (45) for a monotonic function $\kappa(G)$ has a unique solution. Here, we designate $\kappa(G_L)$ as the value of the gray gas absorption coefficient which yields an exact value of the gray gas transmissivity $\tau^{\Delta G}(L)$ for the interval $G_{j-1} < G < G_j$. Then, combining Eqs. (40), (43), and (45), and taking into account the monotonicity of the exponential function, bounds for the optimal value of the gray gas absorption coefficient are obtained

$$\kappa(G_{j-1}) \leq \kappa(G_L) \leq \kappa(G_p) \quad (46)$$

Therefore, the proper choice of the gray gas absorption coefficient κ_j should be in the interval defined by the inequality of Eq. (46). One can confirm with a representative example that the Geometric Mean $\kappa_{GM} = \sqrt{\kappa(G_{j-1}) \kappa(G_j)}$ used to determine the gray gas absorption coefficient satisfies this criterion, but the Arithmetic Mean does not. Indeed, in general,

$$\kappa_{GM} = \sqrt{\kappa(G_{j-1}) \kappa(G_j)} \leq [\kappa(G_{j-1}) + \kappa(G_j)]/2 = \kappa_{AM} \quad (47)$$

Consider the model spectrum reordered absorption coefficient $\kappa(G)$ with a log-uniform dependence on the variable G typical for the real absorption coefficients

$$\kappa(G) = \kappa(G_{j-1}) \left[\frac{\kappa(G_j)}{\kappa(G_{j-1})} \right]^{\frac{G-G_{j-1}}{G_j-G_{j-1}}}, \quad G_{j-1} \leq G \leq G_j \quad (48)$$

for which the analytical calculations can be performed. Now, assume arbitrarily a decade increment between the gray gases (which is reasonably representative of actual RC-SLW calculations)

$$\kappa(G_j) = 10 \kappa(G_{j-1}) \quad (49)$$

Then the upper bound for the optimal local absorption coefficient is

$$\kappa(G_p) = \frac{1}{\Delta G} \int_{\Delta G} \kappa(G) dG = \frac{\kappa(G_j) - \kappa(G_{j-1})}{\ln[\kappa(G_j)/\kappa(G_{j-1})]} \approx 3.9 \kappa(G_{j-1}) \quad (50)$$

and the local absorption coefficients determined with the Geometric Mean and the Arithmetic Mean are

$$\kappa_{GM} = \sqrt{\kappa(G_{j-1}) \kappa(G_j)} \approx 3.16 \kappa(G_{j-1}) \quad (51)$$

$$\kappa_{AM} = [\kappa(G_{j-1}) + \kappa(G_j)]/2 = 5.5 \kappa(G_{j-1}) \quad (52)$$

Therefore, in this example, comparison of values in Eqs. (49) – (52) yields

$$\kappa(G_{j-1}) < \kappa_{GM} < \kappa(G_p) < \kappa_{AM} < \kappa(G_j) \quad (53)$$

This finding is significant, as it defines for the first time the bounding interval for the gray gas absorption coefficient that provides greatest accuracy in RC-SLW model predictions. According to Eq. (53) the use of the Geometric Mean absorption coefficient κ_{GM} always falls within the bounds identified theoretically for the optimal gray gas coefficient. Further, it is seen that the Arithmetic Mean Absorption coefficient κ_{AM} is always outside the bounds for the optimal absorption coefficient (for finite number of gray gases, since all approaches converge to the same gray gas absorption coefficient as $n \rightarrow \infty$). Therefore, the Geometric Mean κ_{GM} is the

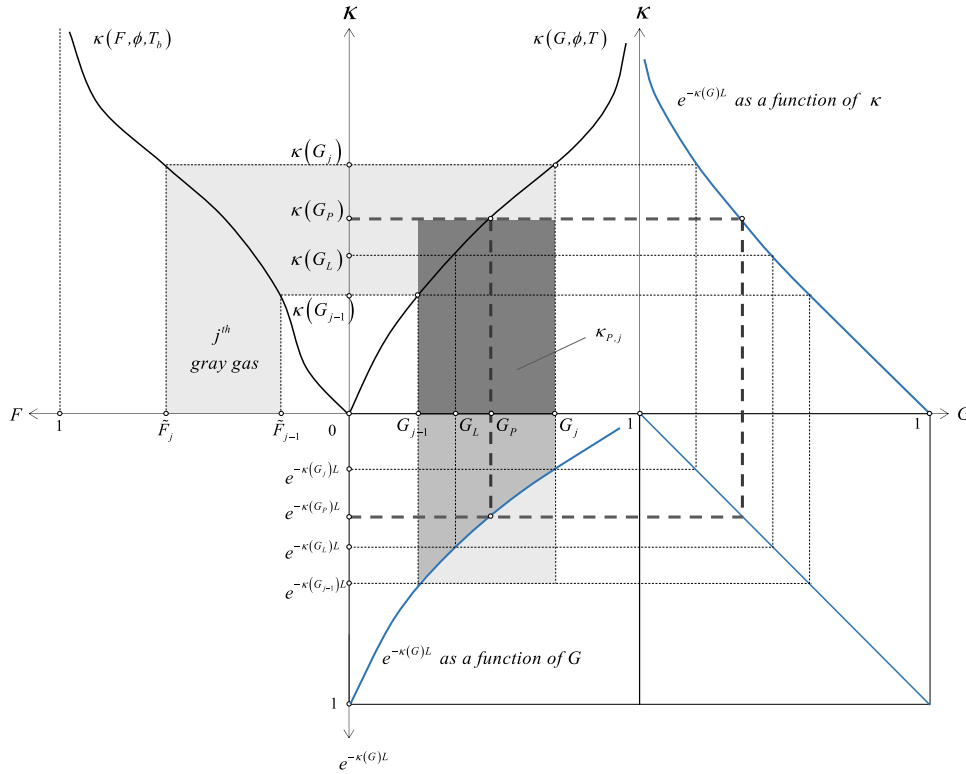


Fig. 8. The bounds of the local gray gas absorption coefficients.

preferred choice for the local gray gas absorption coefficient in RC-SLW modeling, and the Arithmetic Mean κ_{AM} cannot be recommended.

It may also be shown from Eqs. (46) and (53) that the optimal value of the RC-SLW model gray gas absorption coefficient always corresponds to an interval fraction $f < 0.5$ in the supplemental ALBDF interval \tilde{F}_{j-1} to \tilde{F}_j . These conclusions are consistent with the principal findings in the predictions of Tests 1 – 3: i) The Geometric Mean approach for determining the gray gas absorption coefficient, κ_{GM} , is significantly more accurate than the Arithmetic Mean, κ_{AM} , for any number of gray gases; and ii) The optimal value of the gray gas absorption coefficient is always found for a fraction $f < 0.5$ in the interval \tilde{F}_{j-1} to \tilde{F}_j . In the next section a more precise estimate of the local absorption coefficient with respect to the optimal value $\kappa(G_L)$ will be explored.

3.2. Relationship between G_L and the geometric mean

From Eq. (28), the value of the absorption coefficient which yields the exact j^{th} gray gas transmissivity of the pathlength L is

$$\kappa(G_L) = -\frac{1}{L} \ln \left[\frac{1}{G_j - G_{j-1}} \int_{G_{j-1}}^{G_j} e^{-\kappa(G)L} dG \right] \quad (54)$$

One can now denote the ratio of the maximum value to the minimum value of the absorption coefficient in the j^{th} gray gas interval $[\kappa(G_{j-1}), \kappa(G_j)]$ as

$$r = \kappa(G_j) / \kappa(G_{j-1}) \quad (55)$$

Then the assumed log-uniform variation Eq. (48) of the re-ordered absorption coefficient in this interval is written as

$$\kappa(G) = \kappa(G_{j-1}) r^{\frac{G-G_{j-1}}{G_j-G_{j-1}}}, \quad G_{j-1} \leq G \leq G_j \quad (56)$$

The Planck mean gray gas absorption coefficient from Eqs. (44) and (45) is

$$\kappa(G_P) = \frac{1}{G_j - G_{j-1}} \int_{G_{j-1}}^{G_j} \kappa(G) dG = \kappa(G_{j-1}) \frac{r-1}{\ln r} \quad (57)$$

One may now denote the fraction of the interval $[\kappa(G_{j-1}), \kappa(G_P)]$ for the bounds of the exact value $\kappa(G_L)$ estimated by the inequality of Eq. (46) as a function of the pathlength L for different values of r as

$$f_L = \frac{\kappa(G_L) - \kappa(G_{j-1})}{\kappa(G_P) - \kappa(G_{j-1})} \quad (58)$$

The local gray gas absorption coefficient obtained as the Geometric Mean of the values G_{j-1} and G_j is then

$$\kappa_{GM} = \sqrt{\kappa(G_{j-1}) \kappa(G_j)} = \kappa(G_{j-1}) \sqrt{r} \quad (59)$$

Now let the interval fraction $[\kappa(G_{j-1}), \kappa(G_P)]$ associated with the absorption coefficient calculated as the Geometric Mean of the gray gas interval boundary values be

$$f_{GM} = \frac{\kappa_{GM} - \kappa(G_{j-1})}{\kappa(G_P) - \kappa(G_{j-1})} = \frac{(\sqrt{r} - 1) \ln r}{r - 1 - \ln r} \quad (60)$$

Note that this ratio does not depend on pathlength L . A comparison of f_L and f_{GM} as a function of the pathlength L for different values of the ratio r is shown in Fig. 9. In generating this figure, values of $\kappa(G_P)$ were fixed for all curves. The value of $\kappa(G_{j-1})$ was then determined from Eq. (57) for a given r , following which $\kappa(G_j)$ was calculated from Eq. (55). It may be noted that an increase in the number of gray gases corresponds to a decrease in the ratio

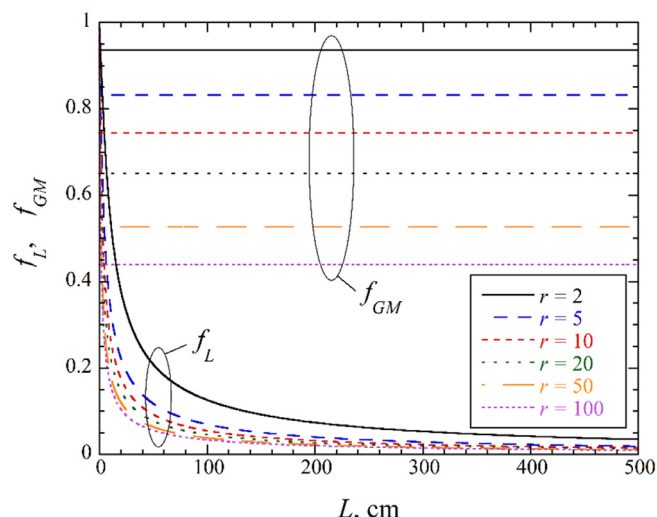


Fig. 9. The interval ratios f_L and f_{GM} as a function of the pathlength L for different values of the ratio r .

$r = \kappa(G_j)/\kappa(G_{j-1})$. As seen in Fig. 9, as $L \rightarrow \infty$, the variable interval fraction corresponding to optimal accuracy approaches $f = 0$, regardless of the interval fraction ratio r used (or alternatively, regardless of the number of gray gases used). For more practical finite values of L (i.e., L neither very large nor very small), Fig. 9 shows that the Geometric Mean provides a value of the local gas absorption coefficient which is always within the bounds defined by Eq. (46) for any value of the ratio $r = \kappa(G_j)/\kappa(G_{j-1})$. The value of gray gas absorption coefficient based on the Geometric Mean is thus always acceptable, with good accuracy confirmed by the test cases presented previously. Further, the results of Fig. 9 confirm the theoretical result derived previously that the optimal gray gas absorption coefficient approaches the minimum value in the interval $G_L \rightarrow G_{j-1}$ corresponding to $f = 0$ as $L \rightarrow \infty$ for any value of r (i.e., any number of gray gases). However, it must be emphasized that for finite pathlengths of interest in most engineering problems, Fig. 9 shows that the optimal value of gray gas absorption coefficient depends on L . This dependence on pathlength makes determination of the optimal gray gas absorption coefficient difficult to generalize. Because the Geometric Mean κ_{GM} always lies in the bounds identified for the optimal gray gas absorption coefficient, it is therefore preferable among all approaches explored, but cannot be considered as the choice yielding exact results for all possible scenarios. This analysis also reveals that further improvement of the RC-SLW spectral model should include consideration of the pathlength L in determining the gray gas absorption coefficient. Finally, note that the exact choice of the absorption coefficient $\kappa(G_L)$ is exact only for prediction of the gray gas transmissivity. It is not necessarily the best choice for prediction of the total divergence of the net radiative flux.

As it follows from this analysis, assuming gray gas coefficients independent of L is probably not optimal, and further, using the minimum value $C_j = \tilde{C}_{j-1}$ is only applicable for very large domain physical lengths. The Geometric Mean approach is the preferred method, since it provides overall the best accuracy at the lowest computational cost. There remains the potential to find an optimum value of the local gray gas absorption coefficient for prediction of the total divergence of the net radiative flux.

4. Conclusions

The sensitivity of the choice of gray gas absorption coefficient in the Rank Correlated SLW model has been explored. Several op-

tions were considered for specifying the gray gas absorption cross-section from the bounding supplemental absorption cross-sections, including i) that determined by inversion of the F -variable using Gauss Quadratures (the original formulation of the RC-SLW method), ii) the Geometric Mean of the bounding values, iii) the Arithmetic Mean, and finally, iv) a value determined from the weighting of the bounding supplemental absorption cross-sections using a variable interval fraction f . It is shown theoretically that an optimal value of the gray gas absorption coefficient can only be determined by accounting for the path length L . However, theory also shows that the optimal choice of gray gas absorption coefficient is always found for an interval fraction $f < 0.5$. Predictions for test cases presented here, confirmed by theoretical foundation, indicates that application of the Geometric Mean of the bounding supplemental absorption cross-sections for the gray gas absorption coefficient is the preferred choice for determining the absorption coefficient compared to the alternatives. In general, this approach results in improved accuracy of prediction of the total divergence of the net radiative flux, and reduces the computation time for construction of the spectral model by a nominal factor of two. The Geometric Mean approach can therefore be considered as an enhancement of the original RC-SLW model formulation. Finally, it is found that for finite number of gray gases, the use of the Arithmetic Mean for calculating the gray gas absorption coefficient is outside the bounds of optimal gray gas absorption coefficient, leading to inaccuracies in the prediction of the local flux divergence. Therefore, the Arithmetic Mean approach is not recommended for use.

Declaration of Competing Interest

The authors declare that they have no known competing financial interests or personal relationships that could have appeared to influence the work reported in this paper.

CRediT authorship contribution statement

Brent W. Webb: Conceptualization, Methodology, Writing – original draft. **Vladimir P. Solovjov:** Conceptualization, Methodology, Software, Writing – original draft. **Frederic André:** Conceptualization, Methodology, Software, Writing – original draft.

References

- [1] Solovjov VP, André F, Lemonnier D, Webb BW. The Rank Correlated SLW model of gas radiation in non-uniform media. *J Quant Spectr Rad Transfer* 2017;197:26–44.
- [2] Solovjov VP, Webb BW, André F. Radiative Properties of Gases. *Handbook of thermal science and engineering*. Kulacki F, editor, New York: Springer; 2018. vol. 2, pp. 1069–1142.
- [3] Webb BW, Solovjov VP, André F. The Spectral Line Weighted-sum-of-gray-gases (SLW) Model for prediction of radiative transfer in molecular gases. *Advances in heat transfer*. Sparrow EM, Abraham JP, Gorman JM, Minkowycz WJ, editors. Academic Press; 2019. vol. 51, pp. 207–298.
- [4] Badger J, Webb BW, Solovjov VP. An exploration of advanced SLW Modeling approaches in comprehensive combustion predictions. *Comb Sci Tech* 2019 <https://doi.org/10.1080/00102202.2019.1678907>.
- [5] Pearson JT, Webb BW, Solovjov VP, Ma J. Efficient representation of the absorption line blackbody distribution function for H₂O, CO₂, and CO at variable temperature, mole fraction, and total pressure. *J Quant Spectr Rad Transfer* 2014;138:82–96.
- [6] Solovjov VP, Webb BW. Multilayer modeling of radiative transfer by SLW and CW methods in non-isothermal gaseous media. *J Quant Spectr Rad Transfer* 2008;109:245–57.
- [7] Solovjov VP, Webb BW. SLW modeling of radiative transfer in multicomponent gas mixtures. *J Quant Spectr Rad Transfer* 2000;65:655–72.
- [8] Solovjov VP, André F, Lemonnier D, Webb BW. The generalized SLW model. *Eurotherm conference 105: computational thermal radiation in participating media V. J. Physics: Conference Series* 2016;012022(676):1–36 2016.
- [9] Webb BW, Solovjov VP, André F. An exploration of the influence of spectral model parameters on the accuracy of the Rank Correlated SLW model. *J Quant Spectr Rad Transfer* 2018;218:161–70.

- [10] Solovjov VP, Webb BW, André F, Lemonnier D. Locally Correlated SLW model for prediction of gas radiation in non-uniform media and its relationship to other global methods. *J Quant Spectr Rad Transfer* 2017;245:26–44.
- [11] Solovjov VP, Webb BW, André F, Lemonnier D. Locally Correlated SLW model for prediction of gas radiation in non-uniform media and its relationship to other global methods. *J Quant Spectr Rad Transfer* 2020;245(106857):1–14.
- [12] André F. Effective scaling factors in non-uniform gas radiation modeling. *J Quant Spectr Rad Transfer* 2018;204:112–19.
- [13] Råde L, Westergren B. *Mathematics handbook for science and engineering*. 4th Ed. NY: Springer; 1999.